

Identification of new OPA1 cleavage site reveals that short isoforms regulate mitochondrial fusion

Ruhan Wang^a, Prashant Mishra^{b,c,d}, Spiros D. Garbis^e, Annie Moradian^e, Michael J. Sweredoski^e, and David C. Chan^{a,*}

^aDivision of Biology and Biological Engineering and ^eProteome Exploration Laboratory of the Beckman Institute, California Institute of Technology, Pasadena, CA 91125; ^bChildren's Medical Center Research Institute, ^cDepartment of Pediatrics, and ^dThe Green Center for Systems Biology, University of Texas Southwestern Medical Center, Dallas, TX 75390

ABSTRACT OPA1, a large GTPase of the dynamin superfamily, mediates fusion of the mitochondrial inner membranes, regulates cristae morphology, and maintains respiratory chain function. Inner membrane-anchored long forms of OPA1 (l-OPA1) are proteolytically processed by the OMA1 or YME1L proteases, acting at cleavage sites S1 and S2, respectively, to produce short forms (s-OPA1). In both mice and humans, half of the mRNA splice forms of *Opa1* are constitutively processed to yield exclusively s-OPA1. However, the function of s-OPA1 in mitochondrial fusion has been debated, because in some stress conditions, s-OPA1 is dispensable for fusion. By constructing cells in which the *Opa1* locus no longer produces transcripts with S2 cleavage sites, we generated a simplified system to identify the new YME1L-dependent site S3 that mediates constitutive and complete cleavage of OPA1. We show that mitochondrial morphology is highly sensitive to the ratio of l-OPA1 to s-OPA1, indicating that s-OPA1 regulates mitochondrial fusion.

Monitoring Editor

Thomas Fox
Cornell University

Received: Sep 22, 2020

Revised: Nov 9, 2020

Accepted: Nov 16, 2020

INTRODUCTION

By controlling mitochondrial form and function, the dynamics processes of mitochondrial fusion and fission regulate cellular physiology, including responses to metabolic demands and cellular stress

This article was published online ahead of print in MBoC in Press (<http://www.molbiolcell.org/cgi/doi/10.1091/mbc.E20-09-0605>) on November 25, 2020.

Conflict of interest: The authors declare they have no conflicts of interest with the contents of this article.

Author contributions: R.W. and D.C.C. conceptualized the project, analyzed the data, and wrote the manuscript. R.W. carried out the experimental analysis. P.M. performed the PA-GFP fusion assays. A.M. performed the LC-MS experiments. The data were analyzed by S.D.G. and M.J.S.

*Address correspondence to: David C. Chan (dchan@caltech.edu).

Abbreviations used: ATP, adenosine triphosphate; CHX, cycloheximide; CRISPR, clustered regularly interspaced short palindromic repeats; GFP, green fluorescent protein; gRNA, guide RNA; GTP, guanosine triphosphate; IM, inner membrane; IRES, internal ribosomal entry site; LC-MS, liquid chromatography-mass spectrometry; MEFs, mouse embryonic fibroblasts; MTS, mitochondrial targeting sequence; N-terminal, amino terminal; OM, outer membrane; OXPHOS, oxidative phosphorylation; SD, standard deviation; SDS-PAGE, sodium dodecyl sulfate polyacrylamide gel electrophoresis; shRNA, short hairpin RNA; WT, wildtype; YFP, yellow fluorescent protein.

© 2021 Wang et al. This article is distributed by The American Society for Cell Biology under license from the author(s). Two months after publication it is available to the public under an Attribution-Noncommercial-Share Alike 3.0 Unported Creative Commons License (<http://creativecommons.org/licenses/by-nc-sa/3.0>).

"ASCB@," "The American Society for Cell Biology@," and "Molecular Biology of the Cell@" are registered trademarks of The American Society for Cell Biology.

(Chan, 2020). As double-membrane organelles, mitochondria fuse by a two-step process coordinated by a set of dynamin superfamily GTPases. In mammalian cells, mitochondrial outer membrane fusion mediated by the mitofusins MFN1 and MFN2 is followed by inner membrane fusion mediated by OPA1 (Chan, 2020). Each of these fusion molecules is essential for embryonic development in mice (Chen et al., 2003; Alavi et al., 2007). In humans, heterozygous mutations in *MFN2* and *OPA1* cause the neurodegenerative diseases Charcot-Marie-Tooth disease 2A and autosomal dominant optic atrophy, respectively (Alexander et al., 2000; Delettre et al., 2000; Chan, 2020).

Owing to alternative splicing and posttranslational processing, the *OPA1* locus gives rise to a complicated set of protein isoforms. In humans, *OPA1* encodes eight mRNA splice forms that are generated by alternative splicing of exons 4, 4b, and 5b (Supplemental Figure S1A). In both humans and mice, the mRNA splice forms are expressed in a tissue-specific manner, although the purpose of this differential expression is unknown (Delettre et al., 2001; Akepati et al., 2008). The encoded OPA1 polypeptides are directed into mitochondria due to an N-terminal mitochondrial targeting sequence (MTS) that is cleaved by the mitochondrial processing peptidase (MPP) soon after entry of this region into the matrix. Lateral exiting of the polypeptide from the TIM (translocase of the inner membrane) pore results in a "long" form of OPA1 (l-OPA1) that is

anchored in the mitochondrial inner membrane by an N-terminal transmembrane segment. A fraction of l-OPA1 is proteolytically cleaved beyond the transmembrane segment by either OMA1 or YME1L, inner membrane-anchored proteases, to produce slightly different, non-membrane-anchored, "short" forms (s-OPA1). OMA1 cleaves at the S1 site encoded by exon 5 (Ehse et al., 2009; Head et al., 2009), and YME1L cleaves at the S2 site encoded by the alternative exon 5b (Griparic et al., 2007; Song et al., 2007). For isoforms 1, 2, 4, and 7, the moderate action of these proteases typically results in roughly comparable levels of long-versus-short OPA1. In contrast, the polypeptides encoded by the other four mRNA splice forms (3, 5, 6, and 8), which all contain exon 4b, are such avid substrates for proteolytic processing that they generate only short forms (Griparic et al., 2007; Song et al., 2007) (Supplemental Figure S1A). Although little detail is available, it has been suggested that exon 4b may encode a protease cleavage site (Olichon et al., 2007; Head et al., 2009; Lee et al., 2017). Under normal conditions, a balanced combination of long and short forms is required to maintain high levels of mitochondrial fusion (Song et al., 2007). Proteolytic processing of the OPA1 orthologue *Mgm1p* is also necessary for normal levels of mitochondrial fusion in yeast cell (DeVay et al., 2009). In contrast, either s-OPA1 or l-OPA1 is sufficient for the non-fusion functions of OPA1, such as maintenance of mitochondrial DNA, cristae structure, and respiratory chain assembly (Del Dotto et al., 2017; Lee et al., 2017).

These observations raise several important issues. How do long and short forms of OPA1 contribute to mitochondrial inner membrane fusion? In particular, what is the purpose of the short forms of OPA1, given that four of eight mRNA splice isoforms give rise to exclusively short forms? There are currently two general models explaining how long and short OPA1 isoforms regulate inner membrane fusion activity. The first model is that a mixture of long and short forms is critical for fusion (Song et al., 2007; Mishra et al., 2014). This model is based on cell culture observations that expression of l-OPA1 or s-OPA1 alone results in very low mitochondrial fusion activity and that robust levels of fusion require a combination of both long and short forms (Song et al., 2007). Furthermore, in an in vitro fusion assay, mitochondria containing l-OPA1 do not fuse until partial proteolytic cleavage is triggered (Mishra et al., 2014). The second model is that l-OPA1 and s-OPA have distinct activities, with l-OPA1 being the only fusogenic form. This model is based on the observation that cells lacking OMA1 and YME1L, which produce only long forms of OPA1, nevertheless show tubular mitochondria and mitochondrial fusion activity (Anand et al., 2014). In addition, under a stress condition termed stress-induced mitochondrial hyperfusion, l-OPA1 is sufficient for fusion activity (Tondera et al., 2009). These observations indicate that under specific cellular conditions, l-OPA1 alone can have substantial fusion activity, even though this does not appear to be the case under basal conditions. S-OPA1 has indeed been suggested to have fission activity, based on the observation that overexpression of s-OPA1 leads to mitochondrial fragmentation (Anand et al., 2014). Recent reconstitution of OPA1 fusion activity in vitro (Ban et al., 2017) has not distinguished between these two models, because both l-OPA1 and s-OPA1 show liposome fusion activity (Ban et al., 2018). However, consistent with the first model, s-OPA1 seems to work synergistically with l-OPA1 to increase in vitro fusion activity (Ban et al., 2017). Observation of single fusion events in another in vitro assay also supports the view that fusion efficiency is increased when a stoichiometric amount of s-OPA1 is added to l-OPA1 (Ge et al., 2020).

To understand the role of the short forms of OPA1, we used CRISPR-Cas9 gene editing to generate cells and mice lacking

OPA1 isoforms containing the YME1L-dependent S2 site encoded by exon 5b. This genetic change eliminated all OPA1 isoforms containing this exon, and we anticipated that the role of YME1L in regulating OPA1 function would be abrogated due to the elimination of the YME1L cleavage site. Surprisingly, however, OPA1 processing was still regulated by YME1L due to a novel cleavage site, which we term S3, encoded by the alternative exon 4b. Notably, isoform 5 contains exon 4b and is constitutively cleaved at S3, and therefore this mRNA isoform contributes only s-OPA1 to the OPA1 repertoire. In specific cellular contexts, we show that depletion of S3-generated s-OPA1 causes mitochondrial fragmentation, and conversely, that increased expression of S3-generated s-OPA1 induces mitochondrial elongation. These results demonstrate that s-OPA1 works with l-OPA1 to tune the level of mitochondrial fusion.

RESULTS

OMA1 and YME1L differentially modulate OPA1 fusion activity

Whereas human OPA1 has eight different mRNA splice variants (Supplemental Figure S1A), mouse tissues express only four—isoforms 1, 5, 7, and 8 (Akepati et al., 2008) (Figure 1A). Each of isoforms 1 and 7 produces a mixture of l-OPA1 and one or two versions of s-OPA1, respectively. The short isoforms are produced by proteolytic cleavage of the long isoform by the mitochondrial inner membrane proteases OMA1 (at the S1 site) and YME1L (at the S2 site). In contrast, proteolytic processing of isoforms 5 and 8 goes to completion and results in only short isoforms (Song et al., 2007).

In mouse embryonic fibroblasts (MEFs), this group of four mRNA isoforms gives rise to five protein bands when cell lysates are resolved on SDS-PAGE (labeled a–e in Figure 1, A and B). Bands a and b are the long forms arising from isoform 7 and isoform 1, respectively (Figure 1A). Bands c and d are S1- and S2-cleavage products of isoform 7 generated by OMA1 and YME1L, respectively. Band e is the short, S1-cleaved form of isoform 1. Isoforms 5 and 8 generate only short isoforms that would be expected to contribute to bands c–e (Song et al., 2007). The same set of OPA1 bands has been observed in other studies, although the relative intensities can vary, perhaps due to differences in culture conditions (Anand et al., 2014).

The dependencies of bands c–e on the OMA1 or YME1L proteases were confirmed by the OPA1 band pattern in lysates from *Oma1*-null or *Yme1L*-null cells (Figure 1B). The OPA1 band patterns observed in the protease mutant cells are tabulated in Supplemental Figure S1B. The identities of the *Oma1*-null and *Yme1L*-null cells were confirmed by Western blotting against the relevant proteases (Supplemental Figure S1C). Notably, there is a longer band emerging in both the *Yme1L*-null and *Yme1L/Oma1*-null cells, likely due to the disruption of YME1L-dependent short isoform formation (i.e., isoform 8).

To understand the role of these proteases in regulating OPA1 fusogenic function, we examined *Oma1/Yme1L* double knockout MEFs, which contain only long forms of OPA1 (Anand et al., 2014). In standard high glucose culture medium, these cells show increased mitochondrial fragmentation compared with wild-type (WT) cells (Figure 1, C and D). Many *Oma1/Yme1L* mutant cells nevertheless show short tubular mitochondria (Figure 1D), so the degree of mitochondrial fragmentation is substantially less severe than in *Mfn1/Mfn2*-null or *Opa1*-null cells (Chen et al., 2005, 2007). *Oma1*-null MEFs show normal mitochondrial morphology profiles, and *Yme1L*-null MEFs show highly fragmented mitochondria (Figure 1D). The overall trends—that mitochondria in *Oma1/Yme1L* mutant cells are more fragmented than in WT cells, but less so than in *Yme1L* mutant cells—are consistent with a previous study (Anand et al., 2014). OPA1

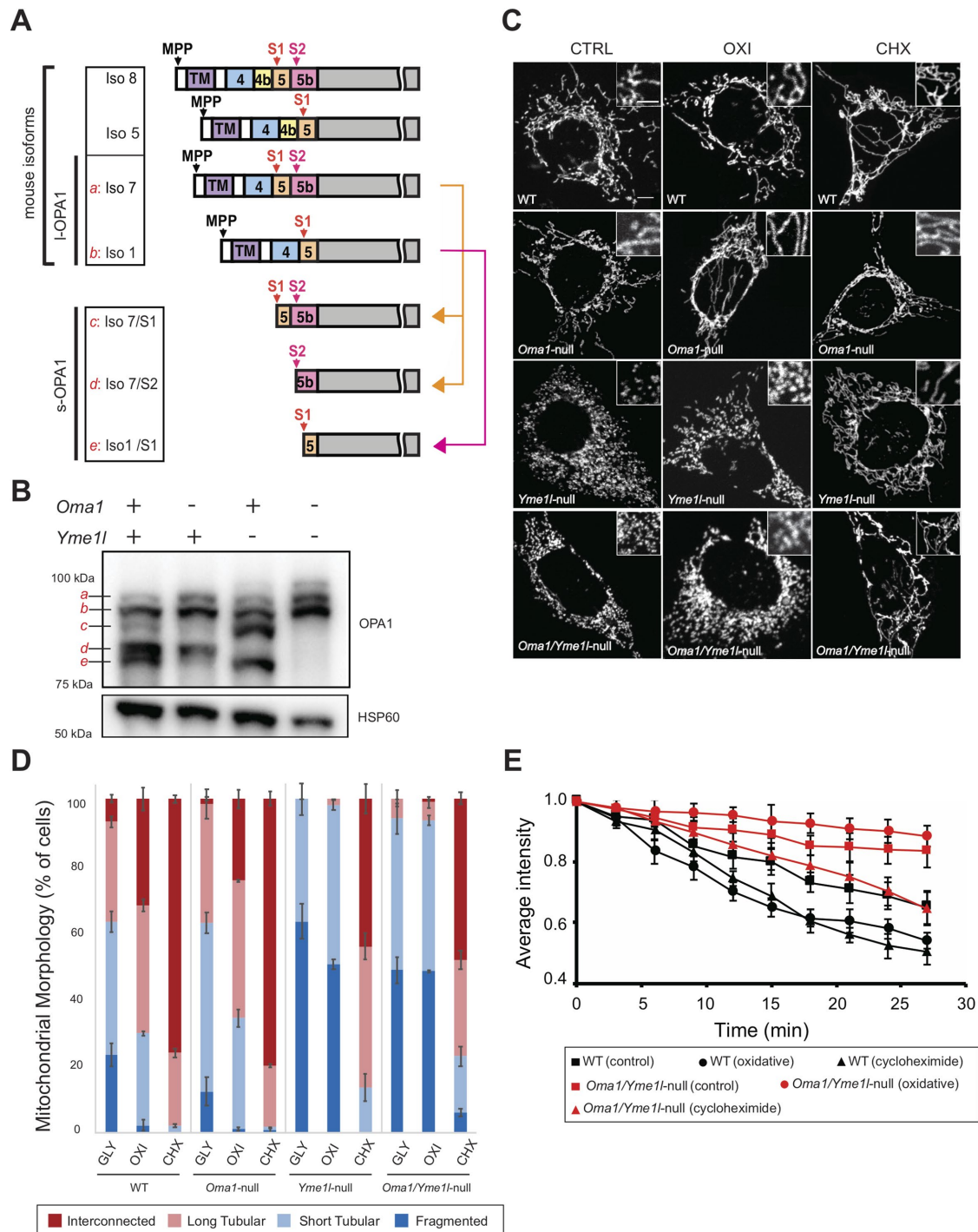


FIGURE 1: OMA1 and YME1L differentially regulate OPA1 fusion activity. (A) Schematic of mouse OPA1 protein isoforms, showing the origin of protein bands a–e. MEFs express isoforms 1, 5, 7, and 8. Isoforms 1 and 7 produce long forms that constitute bands a and b and short forms that constitute bands c–e. Isoforms 5 and 8 produce exclusively short forms expected to comigrate with bands c–e, but for simplicity, bands c–e are labeled according to their origin from isoforms 1 and 7. The MPP (mitochondrial processing peptidase), S1 (by OMA1), and S2 (by YME1L) cleavage sites are indicated with arrows. The orange line and arrows show that bands c and d are derived from long isoform 7/a, and the pink line and arrow show that band e is derived from the long isoform 1/b. (B) Western blot analysis of OPA1 bands in *Oma1* and *Yme1l* mutant MEFs. Five OPA1 bands (a–e) are apparent in wild-type MEFs. *Oma1*-null MEFs lack c and e; *Yme1*-null MEFs lack d; and *Oma1/Yme1*-null MEFs lack all the short forms, c–e. Tubulin was used as loading control. (C) Representative images of mitochondrial morphology (mito-DsRed) in WT and protease-null MEFs in different media. GLY: high glucose medium; OXI: OXPHOS-inducing medium; CHX: high glucose medium with 10 μ M cycloheximide. Insets show magnified view. Scale bar, 5 μ m. (D) Quantification of mitochondrial morphology of cells in C. In each experiment, 100 cells were scored. Error bars show SD from three independent experiments. (E) Comparison of mitochondrial fusion rates in vivo in WT and *Oma1/Yme1*-null MEFs. Fusion activity was measured by the intensity reduction of PA-GFP as a function of time. Error bars represent SDs from at least six independent measurements.

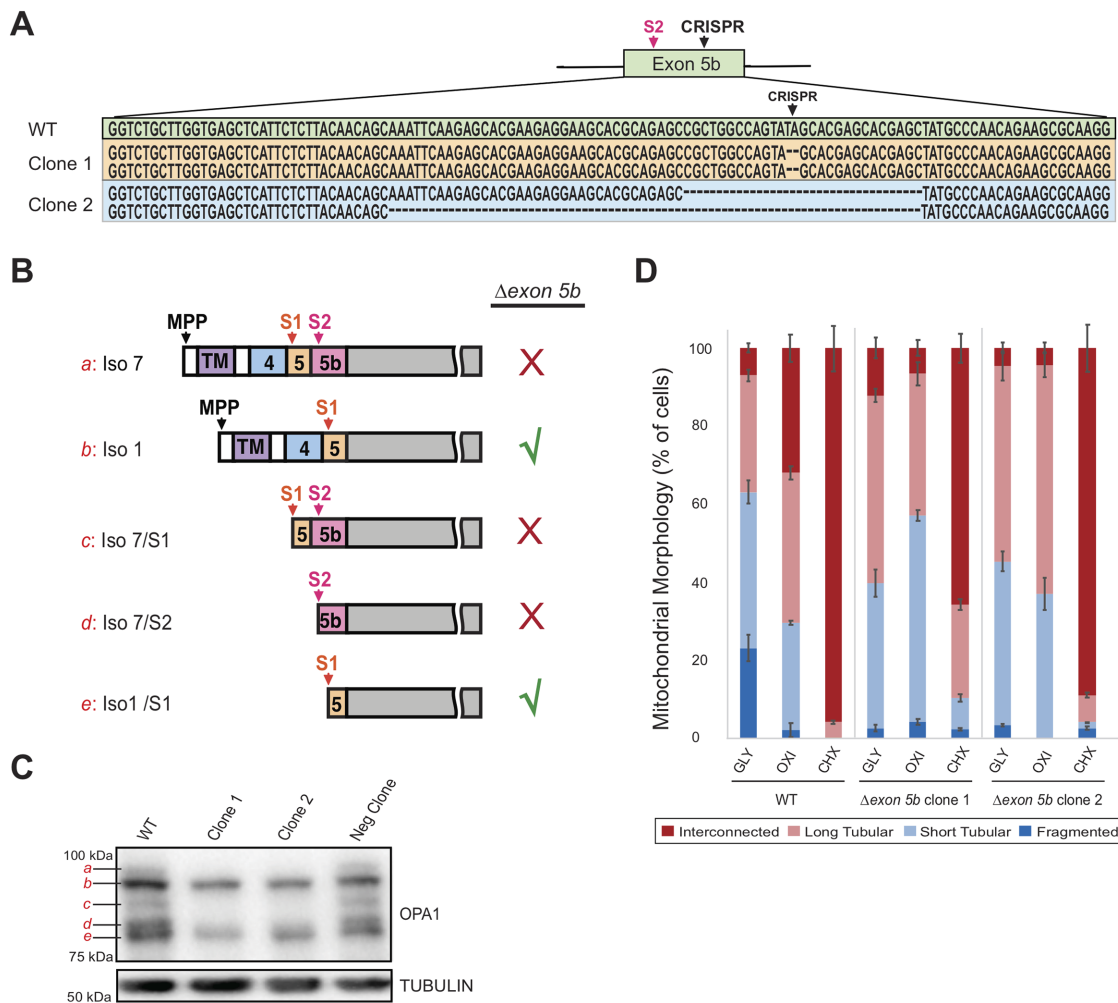


FIGURE 2: The S2 site encoded by *Opa1* exon 5b is necessary for OXPHOS-induced fusion in vivo. (A) Schematic of exon 5b, showing locations of S2 and the CRISPR-Cas9 gRNA target. Deletions present in clones 1 and 2 are indicated. (B) Schematic of OPA1 isoform composition after exon 5b-containing isoforms are eliminated; Red Xs indicate isoforms expected to be missing in mutant cells. (C) Western blot analysis of Δ exon 5b MEF clones. Clones 1 and 2 are positive clones that show the expected disappearance of bands *a*, *c*, and *d*. The last lane is a negative clone. Tubulin was used as loading control. (D) Quantification of mitochondrial morphology in WT and two Δ exon 5b clones in the indicated media. One hundred cells were counted for each experiment. Error bars indicate SD from three independent experiments.

band patterns are similar under the different media conditions (Supplemental Figure S1D).

We tested how these mutant cells respond to culture conditions that increase the level of mitochondrial fusion. Cultured MEFs increase mitochondrial fusion activity and show mitochondrial elongation when cultured in medium that induces oxidative phosphorylation (OXPHOS). This response has been shown to depend on YME1L activity (Mishra *et al.*, 2014). Consistent with this idea, we found mitochondrial elongation caused by OXPHOS-inducing medium to be abrogated in *Yme1*-null and *Oma1/Yme1*-null MEFs (Figure 1, C and D). As measured in the photoactivatable (PA)-green fluorescent protein (GFP) fusion assay, mitochondrial fusion under basal conditions was substantially reduced in *Oma1/Yme1*-null MEFs compared with that in WT cells and did not increase in response to OXPHOS-inducing medium (Figure 1E). In contrast, cells of all genotypes tested in this study show robust mitochondrial elongation in response to cycloheximide (CHX) treatment, which causes stress-induced mitochondrial hyperfusion (Tondera *et al.*, 2009) (Figure 1, C–E). Hyperfusion is induced rapidly after the addition of CHX (Figure 1E). CHX treatment enhanced PA-GFP signal dilution in

both WT and *Oma1/Yme1*-null cells. WT cells showed a substantially greater fusion rate than the latter, indicating the reduced fusion capability in *Oma1/Yme1*-null cells even in the presence of a strong fusion stimulus. Taken together, our observations agree with the previous finding that *Oma1/Yme1*-null cells, containing only I-OPA1, retain mitochondrial fusion activity (Anand *et al.*, 2014). However, the level of fusion activity is substantially lower compared with that in WT cells. The OMA1 and YME1L proteases differentially regulate OPA1 function. Stress-induced hyperfusion does not depend on either protease, consistent with the report that I-OPA1 is sufficient in mediating fusion under this stress condition (Tondera *et al.*, 2009). In contrast, OXPHOS-induced mitochondrial elongation is dependent on YME1L activity, as noted previously (Mishra *et al.*, 2014).

The *Opa1* S2 site is necessary for mediating OXPHOS-induced fusion in vivo

To clarify the functions of YME1L-dependent cleavage of OPA1, we used CRISPR-Cas9-mediated gene targeting in MEFs to generate mutations in the *Opa1* genomic locus at exon 5b, which encodes

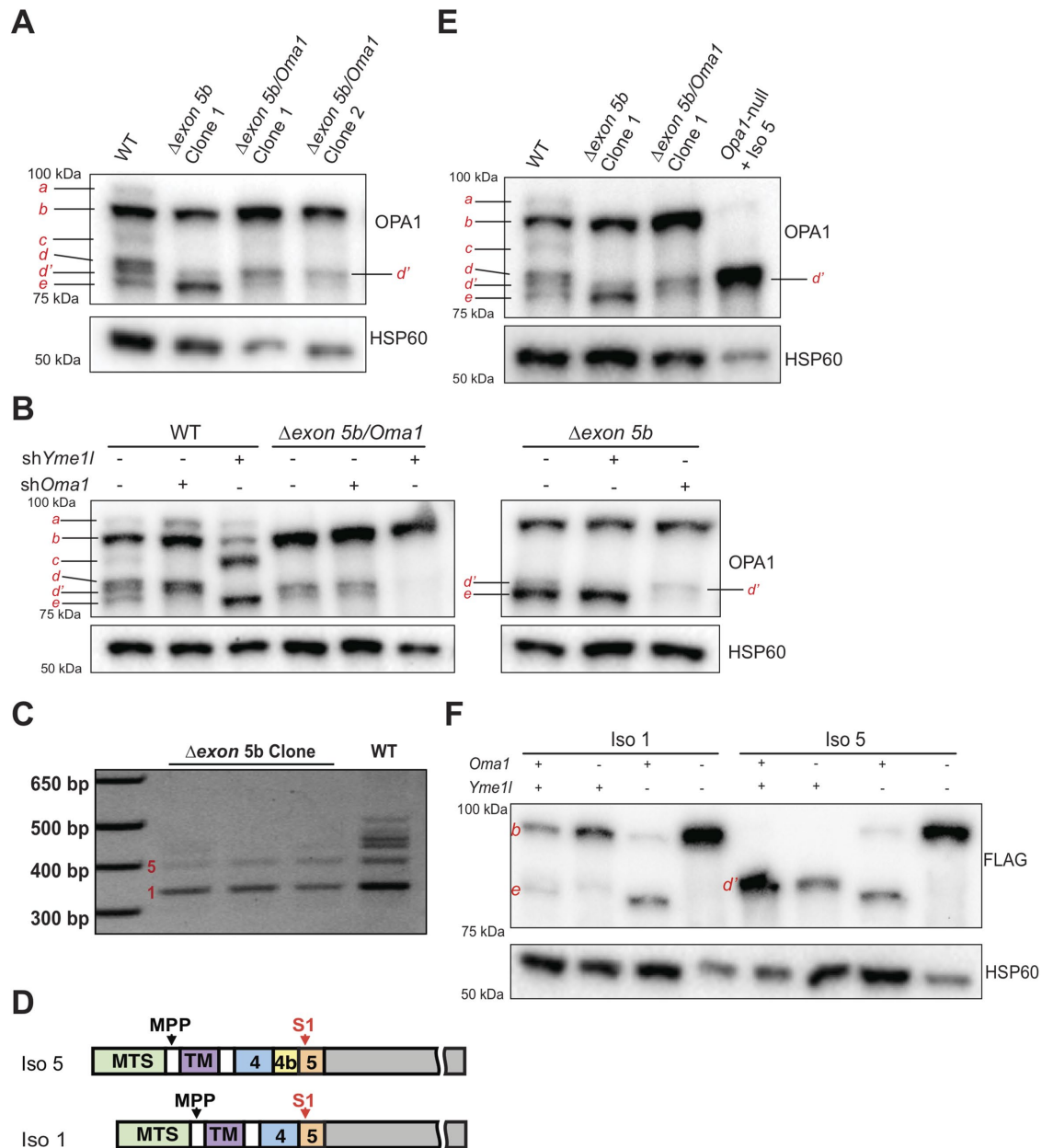


FIGURE 3: Detection of a new OPA1 cleavage in WT and Δ exon 5b cells. (A) Higher-resolution Western analysis of WT, Δ exon 5b, and Δ exon 5b/Oma1-null MEFs. Note the additional band located under d in WT MEFs. This band (referred to as d') is more clearly seen in Δ exon 5b and Δ exon 5b/Oma1-null clones. HSP60 was used as loading control. (B) Dependence of band d' on Yme1l. Cells expressing the indicated shRNA were analyzed by Western blotting. The two sets of panels were run on the same gel. HSP60 was used as loading control. (C) PCR analysis of Opa1 transcripts in Δ exon 5b cells. The forward primer is located in exon 3, and the reverse primer is located in exon 7 (Supplemental Figure S3C). Bands corresponding to isoforms 1 and 5 were confirmed by sequencing. (D) Schematic of full-length OPA1 isoforms 1 and 5. (E) Western blot analysis of the short form produced by isoform 5. HSP60 was used as loading control. (F) Dependence of isoform 5 band d' on YME1L. FLAG-tagged human OPA1 (isoform 1 or 5) was expressed in cells of the indicated genotype and analyzed by Western blotting against FLAG. HSP60 was used as loading control.

the S2 cleavage site (Figure 2, A and B). We hoped to generate deletions in exon 5b that would disrupt the *Opa1* reading frame, resulting in a downstream premature stop codon that would prevent the formation of functional OPA1 isoforms containing S2. In this scenario, the mutant cells would be expected to have only long isoform 1 (band b) and the corresponding S1 cleavage product (band e). Bands a, c, and d would be missing, because they arise from exon 5b-containing transcripts (Figure 2B).

After transient expression of Cas9 and gRNA (guide RNA) against the exon 5b target in MEFs, we identified multiple colonies that lacked bands a, c, and d (Figure 2C). To ensure against clone-specific effects, we used three or more Δ exon 5b clones in all our experiments, and results from two different clones are shown in the figures. DNA sequencing showed that clone 1 has a homozygous two-nucleotide deletion and clone 2 has two longer deletions each causing frameshifting (Figure 2A).

The *Δexon 5b* cells showed normal mitochondrial profiles when grown in regular glucose-containing medium. In addition, they showed a normal stress-induced hyperfusion response, dramatically elongating mitochondria upon CHX stimulation (Figure 2D and Supplemental Figure S2A). In OXPHOS-inducing medium, however, the mutant cells did not show any elongation of mitochondria compared with growth in control medium, indicating that S2-cleavage of Opa1 is required for OXPHOS-induced hyperfusion. Although OXPHOS-inducing medium does not promote mitochondrial elongation in *Δexon 5b* cells, we did not detect physiological consequences. OXPHOS-inducing medium caused upregulation of oxygen consumption in these cells (Supplemental Figure S2B), indicating that the increase in respiratory function is not dependent on mitochondrial elongation. Moreover, both WT cells and *Δexon 5b* cells showed similar cell growth after switching to OXPHOS-inducing medium (Supplemental Figure S2C). In addition to MEFs, we generated two *Δexon 5b* mouse lines. Western analysis of mutant tissues showed abrogation of *Opa1* exon 5b-containing protein bands (Supplemental Figure S2D). Despite this biochemical change in OPA1 isoforms, the mutant mice showed no obvious physiological dysfunction and gained weight normally (Supplemental Figure S2E) for at least 1 yr of age.

Detection of a new OPA1 cleavage site in WT and *Δexon 5b* cells

In the course of this study, we switched to a higher-resolution gel system to study these OPA1 protein isoforms. With this new system, what was previously designated as band *d* in WT cells could be resolved into doublet bands, which we designate as *d* and *d'* (Figure 3A). Upon reanalysis, we realized that *Δexon 5b* cells produce two short *Opa1* bands, *d'* and *e*. With deletion of the YME1L-dependent S2 site, *Δexon 5b* cells would be expected to show only OMA1-mediated processing of OPA1. In *Δexon 5b/Oma1*-null cells, band *e* is missing but *d'* band remains, indicating that it is OMA1-independent (Figure 3A).

Because YME1L is the other known intermembrane protease involved in OPA1 posttranslational processing, we used short hairpin RNA (shRNA) to test whether it is essential for the production of band *d'*. The knockdown efficiencies of the *Yme1l* and *Oma1* shRNAs were confirmed by Western blotting (Supplemental Figure S3, A and B). In WT cells, knockdown of YME1L caused the disappearance of bands *d* and *d'*, whereas knockdown of OMA1 caused the disappearance of bands *c* and *e* (Figure 3B). The dependence of *d'* on YME1L but not OMA1 was further confirmed in both *Δexon 5b/Oma1*-null cells and *Δexon 5b* cells (Figure 3B).

To identify the source of the new short OPA1 band *d'*, we used PCR analysis of cDNA from *Δexon 5b* cells to identify the major remaining *Opa1* mRNA transcripts. Using primers flanking the alternative splicing exons 4, 4b, and 5b to distinguish individual mRNA transcripts (Supplemental Figure S3C), we found that the mutant cells expressed mRNA splice variants 1 and 5 (confirmed by both PCR analysis and sequencing), with isoform 1 being slightly more abundant (Figure 3, C and D). It is not surprising that isoforms 7 and 8 are missing, because they contain exon 5b. Isoform 5 instead contains the alternative exon 4b (Figure 3D), and like other exon 4b-containing isoforms, was previously shown to be constitutively cleaved into a short isoform (Song *et al.*, 2007). The constitutive cleavage of isoform 5 was assumed to occur at the S1 site, the only known cleavage site in this isoform (Song *et al.*, 2007). However, we wondered whether this assumption might be incorrect, because cleavage of isoform 5 at S1 would lead to band *e*, not *d'*. To test whether isoform 5 could generate band *d'*, we expressed isoform 5

in *Opa1*-null cells. Isoform 5 generated a short isoform that was clearly distinct from *e* and comigrated with the *d'* bands present in *Δexon 5b* and *Δexon5b/Oma1*-null cells (Figure 3E). This observation indicates that isoform 5 is the likely source of band *d'*. Its cleavage site is N-terminal to S1, as indicated by the slightly larger size of *d'* compared with *e*.

To determine the protease responsible for cleavage of isoform 5 and further confirm that the YME1L-dependent band *d'* indeed arises from isoform 5, we compared the behavior of C-terminal FLAG-tagged human isoforms 5 and 1 in mutant MEFs lacking OMA1 or YME1L. Consistent with previous studies showing cleavage at S1 by OMA1, isoform 1-FLAG produces a short isoform that is dependent on OMA1 (Figure 3F). When YME1L is absent, more of this short isoform is produced, presumably due to up-regulation of OMA1 activity (Wai *et al.*, 2015). As expected, isoform 5-FLAG is completely processed in control MEFs. The absence of OMA1 does not affect the cleavage pattern, indicating that the production of isoform 5 short form is independent of OMA1 (Figure 3F). The removal of *Yme1l* completely abrogates production of this short form and results in a lower band that comigrates with the short isoform generated from isoform 1 (Figure 3F). In addition, a small amount of the long form, previously absent, is formed. These results indicate that, under normal conditions, isoform 5 is processed to completion at a site upstream of S1, in a YME1L-dependent manner, to produce band *d'*. When YME1L is absent, cleavage is activated at the downstream S1 site. Only the long form is generated from isoform 5 when both OMA1 and YME1L are absent (Figure 3F, last lane). Together, the results suggest that OPA1 isoform 5 is highly susceptible to protease processing, normally by YME1L. In the absence of YME1L, OMA1 processes isoform 5 into S1-cleaved OPA1. No additional proteases are sufficient for isoform 5 cleavage, as indicated by the formation of long isoform 5 when both *Yme1l* and *Oma1* are absent.

Identification of a leucine-rich, YME1L-dependent cleavage site in exon 4b

Our results so far suggest that isoform 5 contains a novel YME1L-dependent cleavage site upstream of S1. To pinpoint the new cleavage site (which we designate as S3), we asked whether cleavage is dependent on exon 4b, the first exon upstream of exon 5. Knockdown of exon 4b with shRNA substantially reduced the intensity of band *d'* in WT, *Δexon 5b*, and *Δexon 5b/Oma1*-null cells (Figure 4A, band *d'* marked with asterisks). This dependence suggests that the cleavage site likely resides in exon 4b. To test this idea, we analyzed the behavior of a series of isoform 5 mutants (Mut 1–9) containing various short deletions within exon 4b (Figure 4B). Mutants 1, 2, and 3, containing deletions in the 5' half of exon 4b, show no defect in isoform 5 cleavage processing, indicating that the first half of exon 4b does not contain the cleavage site (Figure 4C). Mutations 4, 5, and 6 result in small amounts of the long form, which normally is absent. In addition, these mutants show prominent production of band *e*. Mutants 7 and 8 also show the presence of the long form and band *e*. In addition, these mutants show novel cleavage products forming a smear above band *e* (Figure 4C). Mutation 9, which deleted the bridging amino acids between exons 4b and 5, generates band *e* and produces new cleavage products without generating a long form of isoform 5. These results suggest that S3 cleavage is sensitive to mutations in the 3' half of exon 4b, and particularly to mutations (mutants 7 and 8) affecting a stretch of five consecutive leucines (amino acids 199–203 in isoform 5). Interestingly, the most prominent effects of the mutations are in the appearance of the long form and novel cleavage products, rather than in elimination of band *d'*.

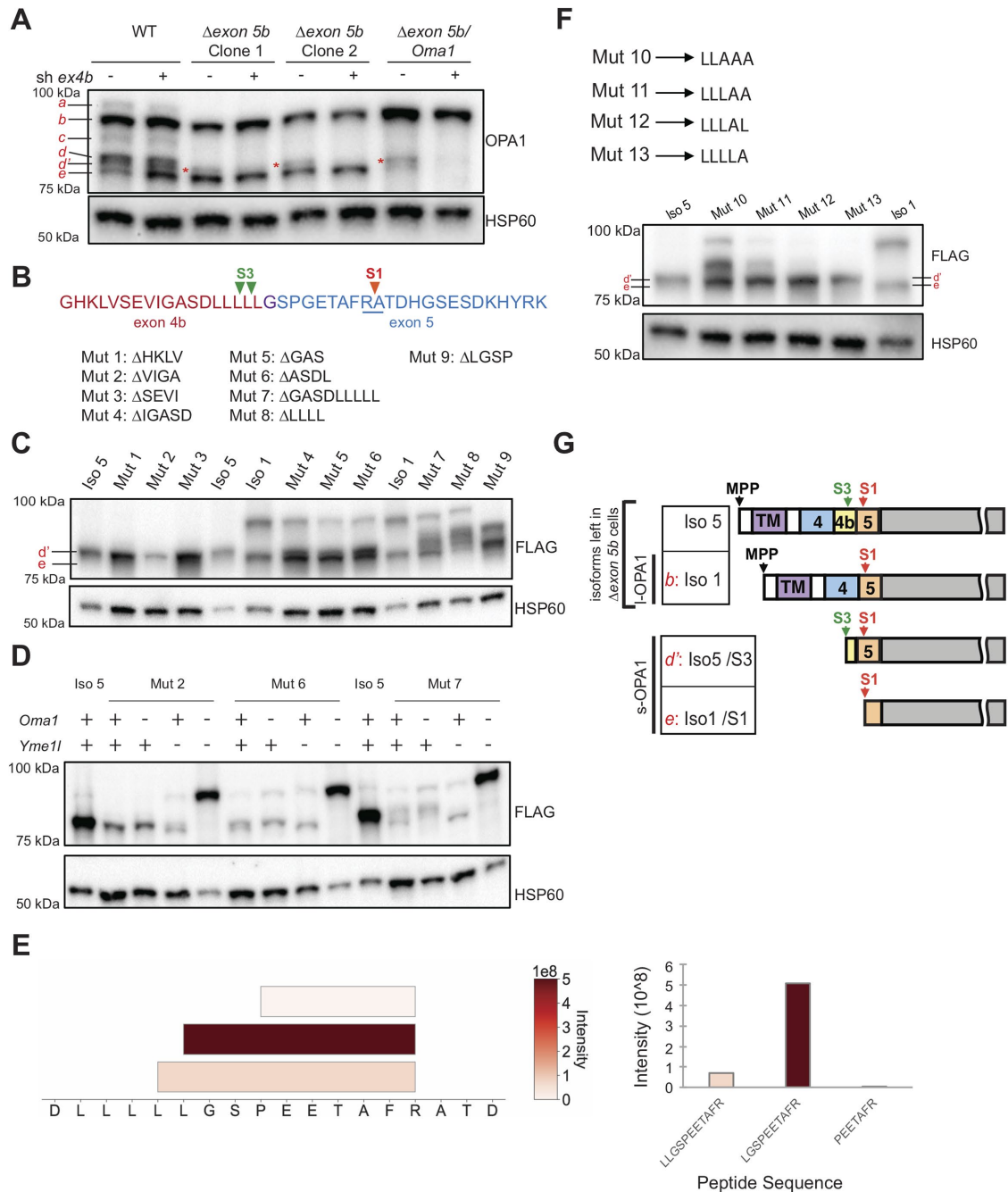


FIGURE 4: Identification of the YME1L-dependent OPA1 S3 cleavage site within exon 4b. (A) Dependence of band *d'* on exon 4b. shRNA against *Opa1* exon 4b was expressed in cells of the indicated genotype. Asterisks highlight band *d'*. HSP60 was used as loading control. (B) Schematic of *Opa1* exon 4b mutants. At the top, the polypeptide sequences encoded by exon 4b (red) and exon 5 (blue) are shown. The red arrow indicates the known S1 cleavage site in exon 5; the green arrows indicate the new S3 sites found in this study. The isoform 5 mutants are listed, along with amino acids deleted within exon 4b. (C) Effect of exon 4b mutants on OPA1 processing. FLAG-tagged exon 4b mutants of human isoform 5 were expressed in *Opa1*-null MEF cells and analyzed by Western blot. FLAG-tagged WT isoforms 1 and 5 were used as controls. HSP60 was used as loading control. (D) Effect of OMA1 and YME1L on OPA1 processing in isoform 5 mutants. WT human Iso 5 and its mutants 2, 6, and 7 were expressed in *Oma1*- and *Yme1l*-null MEFs, and FLAG-tagged OPA1 band patterns were analyzed by Western blot. HSP60 was used as loading control. (E) Identification of likely S3 cleavage sites within exon 4b by tandem mass spectrometry of band *d'*. Band *d'* was produced by expression of FLAG-tagged *Opa1* isoform 5 in 293T cells, purified by anti-FLAG immunoprecipitation, resolved by SDS-PAGE, digested by trypsin, and subjected to tandem mass spectrometry. Left, Schematic indicates the three ragged N-terminal peptides identified, colored according to their relative intensity. Right, Plot of the intensity of the three peptides. (F) Effect of penta-leucine mutants on generation of band *d'*. As indicated, alanines were used to replace 1, 2, or 3 leucines within the C-terminal penta-leucine stretch encoded by exon 4b. FLAG-tagged mutants of isoform 5 were expressed in *Opa1*-null cells and analyzed by Western blot. HSP60 was used as loading control. (G) Schematic of the OPA1 isoform profile in Δ exon 5b MEFs. Green arrow represents the new S3 site identified.

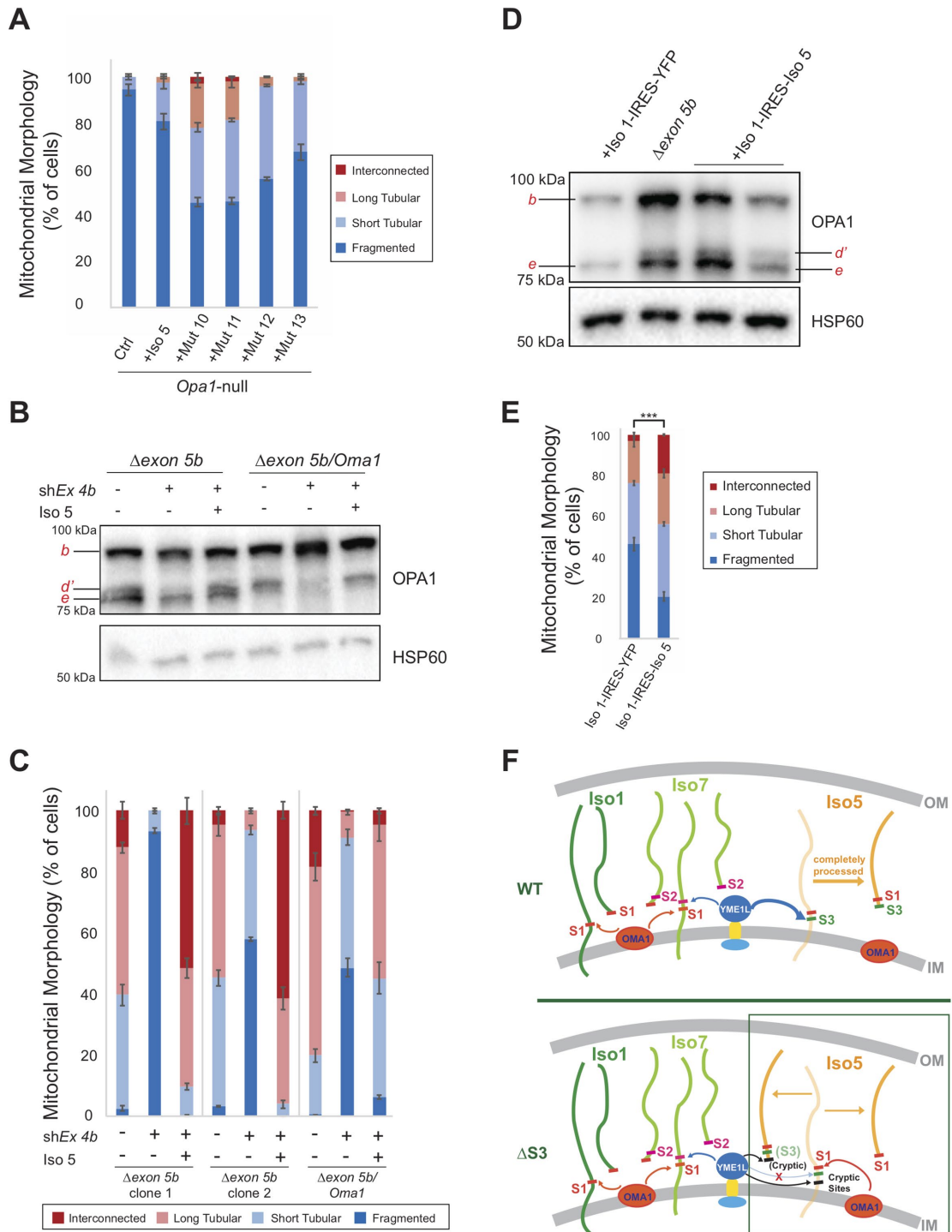


FIGURE 5: The S3-cleaved short form of isoform 5 regulates mitochondrial morphology. (A) Elongation of mitochondria by isoform 5 mutants. Isoform 5 mutants were expressed in *Opa1*-null cells, and mitochondrial morphologies were quantified. Error bars indicate SD from six independent experiments. (B) Depletion of band *d'* by shRNA against exon 4b and reexpression of *d'* by isoform 5. Ectopic expression of isoform 5 is sufficient to overcome the shRNA effect and produce *d'*. OPA1 isoforms were analyzed by Western blotting against OPA1. HSP 60 was used as loading control. (C) Effect of exon 4b shRNA on mitochondrial morphology. Error bars indicate SD from three independent experiments. (D) Analysis of bicistronic OPA1 expression. *Opa1*-null cells expressing isoform 1 or isoform 1 plus isoform 5 were analyzed by Western blotting against OPA1. Δ exon 5b cells are shown for comparison. HSP60 was used as loading control. (E) Effect of band *d'* on mitochondrial morphology. Quantification of mitochondrial morphology of *Opa1*-null MEFs expressing isoform 1 with YFP or isoform 1 with isoform 5. Error bars indicate SD from three independent experiments. *P* values for the fragmented, short tubular, long tubular, and interconnected were 4.8×10^{-4} , 0.04, 0.001, and 9.9×10^{-7} , respectively. *P* values were calculated by Student's *t* test. (F) Model showing the OPA1 isoforms under normal and S3 disrupted conditions. When S3 is disrupted (bottom panel, box), cleavages at S1 and cryptic sites are activated, preserving production of s-OPA1. OM: outer membrane, IM: inner membrane.

To determine the proteases responsible for cleavage of the mutants, we expressed the FLAG-tagged mutants in protease mutant MEFs (Figure 4D). In mutants 6 and 7, the smallest cleavage product disappeared in *Oma1*-null cells, indicating that it is OMA1-dependent. In mutant 7, there are larger short forms that are YME1-dependent. In the absence of both OMA1 and YME1L, no cleavage was observed, demonstrating that these two proteases are essential for isoform 5 processing.

To identify the cleavage site more precisely, we used tandem mass spectrometry to determine the N-terminal sequence of band *d'*, produced by overexpression of FLAG-tagged human isoform 5 in 293T cells. Band *d'* was collected by immunoprecipitation against the FLAG tag, resolved on SDS-PAGE, and isolated for biochemical analysis. Peptides were generated by trypsin digestion and identified by liquid chromatography coupled with nanospray ionization tandem mass spectrometry (LC-MS). Of the peptides identified, only three had nontryptic N-termini. The two predominant ones had N-termini located within exon 4b, beginning with the second to last leucine and last leucine of the penta-leucine stretch (Figure 4E). The latter peptide had by far the highest intensity, suggesting that it represents the predominant S3 cleavage product. To test this idea, we designed isoform 5 mutants (mutants 10–13) in which the last 1–3 leucines of the penta-leucine stretch were substituted with alanine. We found that substitution of a single leucine (mutants 12 and 13) had little effect on band *d'* production, though a small level of larger cleavage products could be observed (Figure 4F). When both of the last two leucines were substituted (mutant 11), there was a more substantial level of aberrant cleavage, and the long isoform appeared. Both these effects were increased when the last three leucines were substituted (mutant 10). Taken together, the LC-MS and mutational analysis strongly argue that the S3 cleavage site lies within the penta-leucine stretch encoded by the end of exon 4b. Although the product ion spectra indicated that cleavage primarily occurs N-terminal to the last leucine, the mutational phenotypes suggest that cleavage can occur at other locations very near the penta-leucine stretch (Figure 4C, lanes 9–13). None of the mutations completely eliminates production of band *d'*, suggesting that cleavage can still occur very close to S3 when the site is mutated. It is also apparent that isoform 5 is highly prone to proteolytic processing—when the S3 site is mutated, cleavage is activated at S1 or at cryptic sites N-terminal to S3, leading to variant cleaved forms of isoform 5. Our analysis indicates that *Δexon5b* cells retain two dominant *Opa1* mRNA transcripts, isoforms 1 and 5. This simplified transcript profile results in one l-OPA1 (from isoform 1) and two s-OPA1 (isoforms 1/ S1 and 5/S3) (Figure 4G).

The S3-cleaved short form of isoform 5 regulates mitochondrial tubulation

In both humans and mice, half of the *Opa1* splice forms contain exon 4b and are constitutively cleaved to yield exclusively short isoforms (Song *et al.*, 2007). This raises the issue of why *Opa1* encodes multiple mRNA splice forms whose only apparent purpose is to generate short isoforms. We used isoform 5 to address this issue. Consistent with previous studies (Song *et al.*, 2007), isoform 5 has almost no mitochondrial elongation activity when expressed in *Opa1*-null MEFs, which have highly fragmented mitochondria due to the complete loss of inner membrane fusion (Figure 5A and Supplemental Figures S5A and S4A). Isoform 5 mutations that disrupt S3 processing, however, show substantial mitochondrial fusion activity, as indicated by their ability to elongate mitochondria (Figure 5A and Supplemental Figures S5A and S4, A and B). Because these mutants produce a variety of short forms as well as a long form,

these results fit with the model that a mixture of long and short isoforms of OPA1 is important for mitochondrial fusion activity (Song *et al.*, 2007). Alternatively, these results could be explained by proposing that it is the production of the long isoform that induces mitochondrial fusion activity.

To distinguish between these two models, we further probed the physiological function of the short form of isoform 5. We used shRNA to knock down exon 4b in *Δexon 5b* and *Δexon 5b/Oma1*-null cells, which have a simplified portfolio of *Opa1* mRNA splice forms. As expected, knockdown of exon 4b resulted in reduction of band *d'* in both cell lines (Figures 4A and 5B). In the *Δexon 5b* MEFs, exon 4b knockdown leads to dramatic mitochondrial fragmentation (Figure 5C and Supplemental Figure S5B). Similarly, in *Δexon 5b/Oma1*-null cells, knockdown of exon 4b results in mitochondrial fragmentation (Figure 5C and Supplemental Figure S5B). To verify that the knockdown result is not due to off-target effects, we reexpressed isoform 5 in the exon 4b knockdowns (Figure 5B) and observed elongation of mitochondrial morphology in both cell lines (Figure 5C and Supplemental Figure S5B).

To further test this idea that a short form of OPA1 can collaborate with a long form to regulate mitochondrial fusion, we developed an expression system to coexpress two different OPA1 splice forms in *Opa1*-null MEFs. We constructed a bicistronic expression vector to generate isoform 1 along with isoform 5, or isoform 1 along with control YFP. Western blot confirmed the expected OPA1 band pattern in these cells (Figure 5D). With isoform 1 expression alone, the long band *b* and the short band *e* were produced. With bicistronic expression of isoforms 1 and 5, an additional short form (*d'* from isoform 5) was added. This dual expression recapitulated the bands observed in *Δexon 5b* cells (Figure 5D) and resulted in longer mitochondrial profiles. Significantly more cells contained interconnected mitochondria, and fewer cells had fragmented mitochondria, compared with the expression of isoform 1 alone (Figure 5E and Supplemental Figure S5C). These results suggest that S3-cleaved s-OPA1 can work with l-OPA1 to promote mitochondrial fusion. To determine whether this synergy requires GTP hydrolysis activity in s-OPA1, we used the bicistronic system to express wild-type isoform 1 with isoform 5 containing a dysfunctional GTPase domain (iso 5-G300E) in *Opa1*-null MEFs. The protein band pattern was similar in cells expressing Iso 1-IRES-Iso 5-G300E compared with cells expressing Iso 1-IRES-Iso 5 (Supplemental Figure S5D). The mutated isoform 5 was ineffective at promoting mitochondrial fusion in combination with wild-type isoform 1, demonstrating that GTPase activity is required in s-OPA1 to maintain fusion function (Supplemental Figure S5, C and E).

DISCUSSION

In this study, we have identified a new site, S3, that is efficiently cleaved by Yme1L to yield s-OPA1. It remains to be determined why YME1L cleaves at S3 much more efficiently than at S2. A short hydrophobic sequence (FAWFP) has been found to act as a degron for YME1L (Shi *et al.*, 2016). However, no similar sequences are apparent in exon 4b or the rest of OPA1. Upon recognition of substrates, YME1L uses ATP hydrolysis to progressively translocate them toward the proteolytic center (Quirós *et al.*, 2015; Puchades *et al.*, 2017). It is plausible that S3, or the region surrounding it, increases the recognition of OPA1 as a Yme1L substrate or its translocation. Future studies can address these issues.

The *OPA1* locus has several mechanisms that safeguard production of s-OPA1. Of the eight *OPA1* mRNA isoforms in humans, four contain exon 4b (Delettre *et al.*, 2001) and encode polypeptides that are fully processed to s-OPA1 (Song *et al.*, 2007). In mice, only four

mRNA isoforms are expressed (Akepati *et al.*, 2008), but similar to humans, half of them contain exon 4b and produce only s-OPA1. With our identification of S3, there are now three cleavage sites that result in the production of s-OPA1 (Figure 5F). This apparent redundancy of sites ensures production of s-OPA1 when one mechanism is disrupted. There is evidence that s-OPA1 is important for cell health, especially under conditions of oxidative stress (Lee *et al.*, 2020).

The redundancy of two YME1L-dependent sites (S2 and S3) likely explains why mice lacking the S2 site do not show obvious physiological abnormalities. In Δ exon 5b mice and cells, RNA isoforms retaining the S3 site are still present and produce sufficient levels of YME1L-dependent s-OPA1 to maintain cellular function. In addition to redundancy of S2 and S3, there appears to be cross-talk between sites to ensure cleavage of OPA1 precursors. With isoform 5, for example, mutation of the S3 site does not abrogate proteolytic processing of OPA1. Rather, it activates OMA1-dependent cleavage at S1 and YME1L-dependent cleavage at upstream cryptic sites, resulting in new short isoforms (Figure 5F). Similarly, mutation of the S1 site activates cryptic cleavage sites (Song *et al.*, 2007). The presence of these multiple mechanisms to generate s-OPA1 suggests that the processed forms likely play an important functional role. It is known that s-OPA1 alone is functional for maintenance of mitochondrial DNA, respiratory complexes, and cristae structure (Del Dotto *et al.*, 2017; Lee *et al.*, 2017), but its role in modulating mitochondrial fusion has been less clear.

Our results support a model in which s-OPA1 collaborates with l-OPA1 to regulate mitochondrial inner membrane fusion. This principle can be readily observed in our engineered cells that have various altered combinations of OPA1 isoforms. In Δ exon 5b/*Oma1*-null cells, only one long form and one short form are produced. Further reduction of s-OPA1 in these cells causes dramatic mitochondrial fragmentation (Figure 5C). Although the long forms by themselves can have fusion activity under certain contexts (mainly the stress-induced hyperfusion condition) (Tondera *et al.*, 2009), l-OPA1 alone is ineffective at maintaining tubular mitochondrial morphology after exon 4b is knocked down in Δ exon 5b/*Oma1*-null cells, which then produce only the long form of isoform 1 (band *b*). Similarly, cells expressing both isoforms 1 and 5 show more tubular mitochondria compared with cells expressing only isoform 1, suggesting that additional production of s-OPA1 in this case promotes mitochondrial fusion (Figure 5E). These results suggest that the ratio of l-OPA1 to s-OPA1 is an important parameter affecting fusion levels.

At present, there is no evidence that the various short forms of OPA1 are functionally distinct with respect to their role in mitochondrial fusion, that is, the slight differences in the lengths of S2-cleaved versus S3-cleaved s-OPA1 probably do not affect their biochemical properties. Our working model is that all the short forms are functionally similar. Mechanistically, the enhancement of tubular mitochondria by s-OPA1 requires its GTP hydrolysis activity (Supplemental Figure S5, C and E), suggesting that it plays an enzymatic role in this process. The multiple cleavage sites allow for production of short forms under basal and stress conditions.

Similar to these results, in two distinct *in vitro* fusion assays, l-OPA1 was sufficient to mediate membrane fusion, but the addition of increasing amounts of s-OPA1 to the same reaction caused higher levels of liposome fusion (Ban *et al.*, 2017; Ge *et al.*, 2020). A previous study suggested that overexpression of s-OPA1 leads to mitochondrial fission, a result interpreted as supporting a role in fission (Anand *et al.*, 2014). We cannot rule out a role of s-OPA1 in fission. However, it is possible that overexpression of s-OPA1 causes an imbalance of the l- to s-OPA1 ratio, which we have shown is critical for

controlling mitochondrial dynamics. Likewise, it has been demonstrated *in vitro* that excessive s-OPA1 in relation to l-OPA1 inhibits membrane fusion (Ge *et al.*, 2020).

It should be noted that the S3 cleavage site we have discovered is a mechanism for constitutive cleavage in OPA1 isoforms containing exon 4b, rather than for induced cleavage under special physiological cues or cellular stress conditions, as is the case for S1 (constitutive and CCCP-inducible). Unlike isoforms containing S1 and S2, which are partially cleaved to generate a cohort of long and short forms, isoforms containing S3 are fully processed under basal conditions to produce solely s-OPA1. The physiological importance of this constitutive cleavage is indicated by our results showing that removal of S3-containing isoforms can cause mitochondrial fragmentation under basal growth conditions.

MATERIALS AND METHODS

Request a protocol through Bio-protocol.

Antibodies

The following antibodies were used: anti-actin (Mab1501R; Millipore), anti-HSP60 (SC-1054; Santa Cruz Biotech), anti-FLAG (F-1804; Sigma), anti-OPA1 (612606; BD Biosciences), anti-TOMM20 (FL-145; Santa Cruz Biotech), anti-TUBULIN (T6199; Sigma), anti-OMA1 (sc-515788; Sigma), and anti-YME1L (11510; Protein Tech Group).

Western blot

A homemade 8% SDS-PAGE gel was used before switching to the high-resolution gel system: The Bio-Rad Mini-PROTEAN precast gel system was used for Western blotting. Ten micrograms of each cell lysate sample was loaded onto 7.5% Mini-PROTEAN TGX precast gels, run at 150 V at 4°C for 2 h to resolve OPA1 bands, and then transferred onto nitrocellulose membranes using Semi-dry Transfer Cell (Bio-Rad), immunoblotted with primary antibodies followed by horseradish peroxidase-conjugated secondary antibodies. Densitometry of Western blots was determined using ImageJ.

Plasmid construction and retroviral transduction

The eight isoforms of human OPA1 cDNA were described previously (Song *et al.*, 2007). FLAG-tagged OPA1 isoforms were constructed by inserting a 3XFLAG sequence (amino acid sequence: DYKDHDGDYKDHDIDYKDDDDK) into the 3' end of the OPA1 gene at the *MfeI/NotI* site. OPA1 sequences are highly similar between mice and humans (Supplemental Figure S4B).

To generate the OPA1 bicistronic expression system, isoform 1 was cloned into pMSCV-IRES-YFP II (Addgene; #52108) at *BamHI/ApaI* sites. Isoform 5 was then cloned into *NcoI/HpaI* sites, replacing YFP.

To generate mutants of OPA1 isoform 5, primers containing deletion mutations were used to amplify 5' and 3' OPA1 fragments, which were then fused together by PCR. The amplified DNA fragments were subcloned back into the pMSCV-Opa1 isoform 5 vector and expressed via retroviral infection.

To disrupt *Opa1* exon 5b, CRISPR-Cas9 sgRNA was analyzed by the online guide RNA (gRNA) design platform at crispr.mit.edu. The gRNA sequence with the highest score was selected and cloned into the pSpCas9n(BB)-2A-Puro plasmid. Transfection and selection were done as previously reported (Ran *et al.*, 2013). The gRNA was generated by the following oligonucleotides:

Forward: CACCGGGGCATAGCTCGTGCTATAC

Reverse: AAACGTATAGCACGAGCTATGCCCC

shRNAs were cloned into the *BglIII/EcoRI* sites of the retroviral vector pRetroX-H1, which contains the H1 promoter. The shRNA target sequences were as follows:

Opa1 exon4b: GGTTAGTGAAGTCCTAGAAGT

Oma1: GCAGTCTACCAGGATAAATCG

Yme1: GCAAATGCTCCTTGTGTATA

Nontargeting: GACTAGAAGGCACAGAGGG

All constructs were authenticated by DNA sequencing.

Mouse breeding

Cas9 mRNA and sgRNA targeting *Opa1* exon 5b were injected into fertilized oocytes at the one-cell stage by the Transgenic/Knockout Rodent Core Facility at USC (University of Southern California). The genotypes of the animals were analyzed by PCR and DNA sequencing, and animals with frameshift mutations were selected. Two homozygous mutant mouse lines—one with a 13-nucleotide deletion and the other with a 44-nucleotide deletion—were found to lack *OPA1* transcripts containing exon 5b. These Δ exon 5b mice were subsequently crossed to *Oma1*-null mice to generate Δ exon 5b/*Oma1*-null animals. Mouse experiments were conducted under protocols approved by the Caltech Institutional Animal Care and Use Committee.

Cell lines and cell culture

MEFs were maintained in DMEM supplemented with 10% fetal bovine serum (FBS) and 1% penicillin/streptomycin at 37°C and 5% CO₂. OXPHOS-inducing medium and glycolytic medium were described previously (Mishra *et al.*, 2014).

The *Opa1*-null, *Oma1*-null, *Yme1*-null, and *Oma1/Yme1*-null MEFs were described previously (Song *et al.*, 2007; Anand *et al.*, 2014). To generate Δ exon 5b MEFs, WT MEFs were transiently transfected with the CRISPR-Cas9 plasmid. Twenty-four hours later the transfected MEFs were selected with 1 μ M puromycin for 24 h, and cells were cloned by limiting dilution in 96-well plates. After expansion, the clones were lysed with RIPA buffer (ThermoFisher Scientific) and analyzed by Western blotting against *OPA1*. Clones with the expected *OPA1* band pattern were expanded, and their genotypes were confirmed by DNA sequencing.

To generate Δ exon 5b/*Oma1*-null fibroblasts, cells were isolated from Δ exon 5b/*Oma1* mouse tails at postnatal day 21 and grown in DMEM supplemented with 10% FBS, essential amino acids, and penicillin/streptomycin at 37°C and 5% CO₂. The fibroblasts were immortalized by expression of SV40 large T antigen. The genotype of the cells was confirmed by PCR and immunoblotting.

Cell respiration measurement

The oxygen consumption rate was measured in a Seahorse Biosciences Extracellular Flux Analyzer (model XF96), as described previously (Mishra *et al.*, 2014).

Imaging and quantification

All images were acquired with a Zeiss LSM 710 confocal microscope with a Plan-Apochromat 63X/1.4 oil objective. Alexa 488- and Alexa 546-conjugated dyes were excited by the 488 nm laser and the 561 nm laser, respectively. Mitochondria were visualized and imaged by immunostaining with Tom20 antibody.

To determine mitochondrial fusion activity, cells were visually scored under a fluorescence microscope (Axiovert 200M; Carl Zeiss MicroImaging) into four morphological classifications. Scoring was done manually, blinded. "Fragmented" refers to cells that contain

spherical mitochondrial fragments with no more than two short tubules found. "Short tubular" refers to cells with a mixture of fragmented and short tubular mitochondria. "Long tubular" refers to cells in which mitochondria were elongated, but not highly interconnected into a mitochondrial mesh. "Interconnected" refers to cells in which mitochondria formed a highly interconnected network of mitochondrial filaments, with few isolated mitochondria. All data are presented as mean \pm SD unless otherwise noted. Quantitative data were analyzed by Student's *t* test for the comparison between two groups (two tailed, unpaired).

PA-GFP fusion assay

Cells expressing matrix DsRed and photoactivatable GFP (PA-GFP) targeted to either the OM or matrix were plated on glass coverslips and imaged live at 37°C on an LSM 710 confocal microscope (Carl Zeiss). Measurements were initiated 1–2 h after medium change. PA-GFP was photoactivated in a region of interest (5 μ m \times 5 μ m) by illumination with a 405 nm laser. The activated fluorescent signal was then collected (for the entire cell) every 3 min for the next 30 min using a spectral detector, followed by spectral unmixing based on the individual PA-GFP and DsRed spectra. Fusion events result in the dilution of the activated signal. The average pixel intensity (for the entire cell) over time is a measurement of fusion rates (Karbowski *et al.*, 2014). Images were analyzed in MatLab (Mathworks). *P* values were calculated using a Student's *t* test on the slopes of intensity versus time for individual measurements (>20 per condition).

Mass spectrometry

At 48 h after transient transfection of FLAG-tagged isoform 5 in 293T cells, cell lysates were harvested and immune precipitated against FLAG. Concentrated samples were run on SDS-PAGE, and colloidal Coomassie blue stain (Invitrogen) was used to identify the bands. The desired bands were excised, finely diced, and transferred to a microcentrifuge tube. The gel pieces were reduced, alkylated, and digested by trypsin overnight at 37°C. Digested peptides were extracted from the gel, lyophilized, and desalted by C18 ZipTips (EMD Millipore). The peptides were separated with a 60 min gradient at a flow rate of 220 nl/min using a nanoflow LC system, EASY-nLC 1000 (ThermoFisher Scientific). The separated peptides were ionized by a Nanospray Flex ion source and subjected to MS/MS analysis using a Fusion Orbitrap mass spectrometer (ThermoFisher Scientific). For LC-MS/MS data analysis, the Thermo raw data file was converted to an mzML file using MSconvert. The mzML file was searched using MS-GF+ against the *Opa1* sequence. Default options were used except precursor mass tolerance was set to 7 ppm, instrument was specified to "Orbitrap/FTICR/Lumos" (1), and enzyme was "Unspecific cleavage" (0). Results were further refined by filtering out all peptide-spectrum matches with an *E* value greater than 0.001.

ACKNOWLEDGMENTS

We thank Thomas Langer (Max-Planck-Institute for Biology of Ageing) for the *Oma1*-null, *Yme1*-null, and *Oma1/Yme1*-null cells. We thank Carlos López Otín (Universidad de Oviedo) for the *Oma1* knockout mice. This work was supported by a grant to D.C.C. from the National Institute of General Medical Sciences (R35GM127147).

REFERENCES

Akepati VR, Müller E-C, Otto A, Strauss HM, Portwich M, Alexander C (2008). Characterization of *OPA1* isoforms isolated from mouse tissues. *J Neurochem* 106, 372–383.

- Alavi MV, et al. (2007). A splice site mutation in the murine Opa1 gene features pathology of autosomal dominant optic atrophy. *Brain* 130, 1029–1042.
- Alexander C, et al. (2000). OPA1, encoding a dynamin-related GTPase, is mutated in autosomal dominant optic atrophy linked to chromosome 3q28. *Nat Genet* 26, 211–215.
- Anand R, Wai T, Baker MJ, Kladt N, Schauss AC, Rugarli E, Langer T (2014). The i-AAA protease YME1L and OMA1 cleave OPA1 to balance mitochondrial fusion and fission. *J Cell Biol* 204, 919–929.
- Ban T, Ishihara T, Kohno H, Saita S, Ichimura A, Maenaka K, Oka T, Mihara K, Ishihara N (2017). Molecular basis of selective mitochondrial fusion by heterotypic action between OPA1 and cardiolipin. *Nat Cell Biol* 19, 856–863.
- Ban T, Kohno H, Ishihara T, Ishihara N (2018). Relationship between OPA1 and cardiolipin in mitochondrial inner-membrane fusion. *Biochim Biophys Acta Bioenerg* 1859, 951–957.
- Chan DC (2020). Mitochondrial dynamics and its involvement in disease. *Annu Rev Pathol* 15, 235–259.
- Chen H, Chomyn A, Chan DC (2005). Disruption of fusion results in mitochondrial heterogeneity and dysfunction. *J Biol Chem* 280, 26185–26192.
- Chen H, Detmer SA, Ewald AJ, Griffin EE, Fraser SE, Chan DC (2003). Mitofusins Mfn1 and Mfn2 coordinately regulate mitochondrial fusion and are essential for embryonic development. *J Cell Biol* 160, 189–200.
- Chen H, McCaffery JM, Chan DC (2007). Mitochondrial fusion protects against neurodegeneration in the cerebellum. *Cell* 130, 548–562.
- Del Dotto V, et al. (2017). OPA1 isoforms in the hierarchical organization of mitochondrial functions. *Cell Rep* 19, 2557–2571.
- Delettre C, et al. (2000). Nuclear gene OPA1, encoding a mitochondrial dynamin-related protein, is mutated in dominant optic atrophy. *Nat Genet* 26, 207–210.
- Delettre C, Griffoin JM, Kaplan J, Dollfus H, Lorenz B, Faivre L, Lenaers G, Belenguer P, Hamel CP (2001). Mutation spectrum and splicing variants in the OPA1 gene. *Hum Genet* 109, 584–591.
- DeVay RM, Dominguez-Ramirez L, Lackner LL, Hoppins S, Stahlberg H, Nunnari J (2009). Coassembly of Mgm1 isoforms requires cardiolipin and mediates mitochondrial inner membrane fusion. *J Cell Biol* 186, 793–803.
- Ehres S, Raschke I, Mancuso G, Bernacchia A, Geimer S, Tondera D, Martinou J-C, Westermann B, Rugarli E, Langer T (2009). Regulation of OPA1 processing and mitochondrial fusion by m-AAA protease isoenzymes and OMA1. *J Cell Biol* 187, 1023–1036.
- Ge Y, Shi X, Boopathy S, McDonald J, Smith AW, Chao LH (2020). Two forms of Opa1 cooperate to complete fusion of the mitochondrial inner-membrane. *eLife* 9, e50973.
- Griparic L, Kanazawa T, van der Bliek AM (2007). Regulation of the mitochondrial dynamin-like protein Opa1 by proteolytic cleavage. *J Cell Biol* 178, 757–764.
- Head B, Griparic L, Amiri M, Gandre-Babbe S, van der Bliek AM (2009). Inducible proteolytic inactivation of OPA1 mediated by the OMA1 protease in mammalian cells. *J Cell Biol* 187, 959–966.
- Karbowski M, Cleland MM, Roelofs BA (2014). Photoactivatable green fluorescent protein-based visualization and quantification of mitochondrial fusion and mitochondrial network complexity in living cells. *Methods Enzymol* 547, 57–73.
- Lee H, Smith SB, Sheu S-S, Yoon Y (2020). The short variant of optic atrophy 1 (OPA1) improves cell survival under oxidative stress. *J Biol Chem*, jbc.RA119.010983.
- Lee H, Smith SB, Yoon Y (2017). The short variant of the mitochondrial dynamin OPA1 maintains mitochondrial energetics and cristae structure. *J Biol Chem* 292, 7115–7130.
- Mishra P, Carelli V, Manfredi G, Chan DC (2014). Proteolytic cleavage of Opa1 stimulates mitochondrial inner membrane fusion and couples fusion to oxidative phosphorylation. *Cell Metab* 19, 630–641.
- Olichon A, Elachouri G, Baricault L, Delettre C, Belenguer P, Lenaers G (2007). OPA1 alternate splicing uncouples an evolutionary conserved function in mitochondrial fusion from a vertebrate restricted function in apoptosis. *Cell Death Differ* 14, 682–692.
- Puchades C, Rampello AJ, Shin M, Giuliano CJ, Wiseman RL, Glynn SE, Lander GC (2017). Structure of the mitochondrial inner membrane AAA+ protease YME1 gives insight into substrate processing. *Science* 358, eaao0464.
- Quirós PM, Langer T, López-Otín C (2015). New roles for mitochondrial proteases in health, ageing and disease. *Nat Rev Mol Cell Biol* 16, 345–359.
- Ran FA, Hsu PD, Wright J, Agarwala V, Scott DA, Zhang F (2013). Genome engineering using the CRISPR-Cas9 system. *Nat Protoc* 8, 2281–2308.
- Shi H, Rampello AJ, Glynn SE (2016). Engineered AAA+ proteases reveal principles of proteolysis at the mitochondrial inner membrane. *Nat Commun* 7, 13301.
- Song Z, Chen H, Fiket M, Alexander C, Chan DC (2007). OPA1 processing controls mitochondrial fusion and is regulated by mRNA splicing, membrane potential, and Yme1L. *J Cell Biol* 178, 749–755.
- Tondera D, et al. (2009). SLP-2 is required for stress-induced mitochondrial hyperfusion. *EMBO J* 28, 1589–1600.
- Wai T, García-Prieto J, Baker MJ, Merkwirth C, Benit P, Rustin P, Rupérez FJ, Barbas C, Ibañez B, Langer T (2015). Imbalanced OPA1 processing and mitochondrial fragmentation cause heart failure in mice. *Science* 350, aad0116.